
Deep Multiple Instance Learning with Distance-Aware Self-Attention

Georg Wölflein
School of Computer Science
University of St Andrews
georg@woelflein.de

Lucie Charlotte Magister
Department of Computer Science and Technology
University of Cambridge
lcm67@cam.ac.uk

Pietro Liò
Department of Computer Science and Technology
University of Cambridge
pl219@cam.ac.uk

David J. Harrison
School of Medicine
University of St Andrews
david.harrison@st-andrews.ac.uk

Ognjen Arandjelović
School of Computer Science
University of St Andrews
oa7@st-andrews.ac.uk

Abstract

Traditional supervised learning tasks require a label for every instance in the training set, but in many real-world applications, labels are only available for collections (bags) of instances. This problem setting, known as multiple instance learning (MIL), is particularly relevant in the medical domain, where high-resolution images are split into smaller patches, but labels apply to the image as a whole. Recent MIL models are able to capture correspondences between patches by employing self-attention, allowing them to weigh each patch differently based on all other patches in the bag. However, these approaches still do not consider the relative spatial relationships between patches within the larger image, which is especially important in computational pathology. To this end, we introduce a novel MIL model with distance-aware self-attention (DAS-MIL), which explicitly takes into account relative spatial information when modelling the interactions between patches. Unlike existing relative position representations for self-attention which are discrete, our approach introduces continuous distance-dependent terms into the computation of the attention weights, and is the first to apply relative position representations in the context of MIL. We evaluate our model on a custom MNIST-based MIL dataset that requires the consideration of relative spatial information, as well as on CAMELYON16, a publicly available cancer metastasis detection dataset, where we achieve a test AUROC score of 0.91. On both datasets, our model outperforms existing MIL approaches that employ absolute positional encodings, as well as existing relative position representation schemes applied to MIL. Our code is available at <https://anonymous.4open.science/r/das-mil>.

1 Introduction

Multiple instance learning (MIL) [1, 2] is a supervised learning framework for data that is supplied as bags of instances, where only the bag labels are known. It has been used in various domains such as image classification [3], object detection [4], drug discovery [5], and text categorization [6]. Recently,

MIL has attracted a lot of attention in the medical imaging community, where it has become the predominant paradigm for classifying whole slide images (WSIs) [7–10]. These are high-resolution, digitised microscopic images of tissue sections which, due to their large size, need to be divided into smaller patches to be processed by deep learning models. Labels are only available at the bag level, *i.e.* for the entire WSI, and not for individual instances (patches).

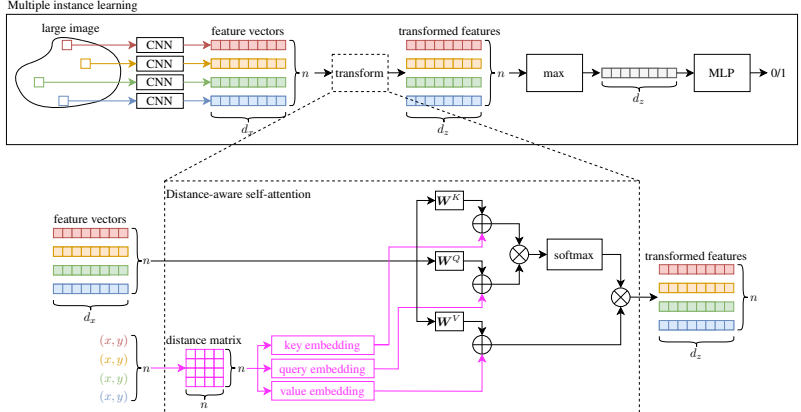


Figure 1: We propose a MIL pipeline (top) with a novel self-attention mechanism (bottom), incorporating relative distance information (magenta) in the computation of the attention weights. A standard MIL assumption in binary classification is that at least one instance per positive bag has the target property, while all instances in negative bags lack it. For example, in classifying WSIs as cancerous or non-cancerous, the assumption is that a cancerous WSI has at least one patch containing tumour tissue, while a non-cancerous WSI does not contain any tumour tissue. A naïve approach is to apply a standard classifier to each instance independently and then aggregate the predictions to obtain the bag-level prediction. However, previous work has shown that this approach runs into the problem of insufficiently training the instance-level classifier due to incorrect instance-level labels [11, 12]. Instead, we focus on the generally preferred embedding-level approach, where the instances are first embedded into a common space and then aggregated to obtain the bag-level prediction [11, 12].

Embedding-level MIL models [11, 12] still operate on the classical MIL assumption that the instances within a bag are independent and that the bag-level prediction can be obtained by aggregating the instance-level predictions. However, this assumption does not always hold in real-world applications such as medical imaging, where instances may exhibit complex dependencies.

Self-attention mechanisms [13] have shown great success in various natural language processing and computer vision tasks because they are able to weigh parts of an input sequence differently based on the entire sequence. In an attempt to weaken the independence assumption in MIL, recent works have proposed to use self-attention in the aggregation step [14–25] because this allows the model to weigh each instance differently based on all other instances in the bag.

In this paper, we study a special case of MIL where instances are equipped with a distance metric. This problem setting arises naturally in the medical imaging domain, where high-resolution histological images are split into smaller patches, and distances between patches can be defined as the Euclidean distance between their centroid coordinates. However, current MIL models, even those employing self-attention in the embedding space [14–25], do not consider the relative distances between instances, which may be important for the classification task. For example, in the computational pathology domain, the spatial relationships between various tissue structures have been shown to be of prognostic value, reflecting the importance of direct cell-cell interactions in influencing biological behaviour [26–28]. Furthermore, the interaction between tumour cells and immune cells, which is inherently spatial in nature, is a factor that may be pivotal in predicting the response to immunotherapy [29, 30].

To address this problem, we introduce a novel MIL model with distance-aware self-attention (DAS-MIL), which explicitly takes into account the pairwise distances between instances in a bag when computing the attention weights (see Fig. 1). To the best of our knowledge, our approach is the first to use relative position representations in MIL, and in the context of relative position representations, the first to use a continuous distance-dependent bias term in the self-attention mechanism. We evaluate our model on a custom dataset requiring distance awareness for prediction, as well as CAMELYON16 [31], a publicly available dataset for cancer metastasis detection.

The remainder of this paper is organized as follows. In Section 2, we review related work, before we introduce our DAS-MIL model in Section 3. In Section 4, we then report experimental results, before we conclude the paper in Section 5 and discuss future directions of research.

2 Background and Related Work

2.1 Multiple instance learning

In the binary MIL setting, the goal is to predict the label $Y \in \{0, 1\}$ of a bag \mathbf{X} of instances $\{\mathbf{x}_1, \mathbf{x}_2, \dots, \mathbf{x}_n\}$ with each instance $\mathbf{x}_i \in \mathbb{R}^n$. Note that the number of instances in a bag, n , may vary. The challenge is that only the bag-level label Y is known and not the corresponding instance-level labels $\{y_1, y_2, \dots, y_n\}$, each $y_i \in \{0, 1\}^n$. However, it can be assumed that there exists at least one positive instance per positive bag, while all instances in negative bags are negative, *i.e.*,

$$Y = \begin{cases} 1 & \text{iff } \sum_{i=1}^{n_i} y_i > 0 \\ 0 & \text{otherwise} \end{cases}. \quad (1)$$

Our training dataset consists of N bags $\mathbf{X}^{(i)}$ with corresponding labels $Y^{(i)}$ for $i = 1, 2, \dots, N$, where each bag $\mathbf{X}^{(i)}$ contains n_i instances $\{\mathbf{x}_1^{(i)}, \mathbf{x}_2^{(i)}, \dots, \mathbf{x}_{n_i}^{(i)}\}$. However, to ease notation, we omit the bag index i , as it is clear from the context that we are referring to some bag \mathbf{X} with associated label Y . It is worth noting, that originally instances within each bag were assumed to be independent and identically distributed (i.i.d.) [1, 2], but recent works have recognised this assumption to often be violated in real-world applications [14, 20].

A MIL learns a scoring function $S : \mathbb{R}^{n \times d_x} \rightarrow \mathbb{R}$ that predicts the bag label Y from the bag \mathbf{X} :

$$\hat{Y} = S(\mathbf{X}) \quad (2)$$

We can decompose the scoring function into three parts. First, a transformation $\mathbf{h} : \mathbb{R}^{d_x} \rightarrow \mathbb{R}^{d_z}$ computes an embedding vector \mathbf{z}_i of dimensionality d_z for each instance \mathbf{x}_i in our bag \mathbf{X} . Then, an aggregation function $\mathbf{g} : \mathbb{R}^{n \times d_z} \rightarrow \mathbb{R}^{d_z}$ combines all the embeddings to a single embedding vector which is finally passed through a classifier $f : \mathbb{R}^{d_z} \rightarrow \mathbb{R}$ to obtain the bag-level prediction:

$$\mathbf{z}_i = \mathbf{h}(\mathbf{x}_i) \quad (3)$$

$$\mathbf{z}' = \mathbf{g}(\{\mathbf{z}_1, \mathbf{z}_2, \dots, \mathbf{z}_n\}) \quad (4)$$

$$S(\mathbf{X}) = f(\mathbf{z}'). \quad (5)$$

As a basic example, one could parameterize f and \mathbf{h} using neural networks and employ the mean function as the aggregation function \mathbf{g} .

Attention-based MIL A popular approach to MIL known as att-MIL employs a simple attention mechanism in the aggregation function [12]. Instead of using the mean function, att-MIL independently computes an individual attention weight α_i for each instance \mathbf{x}_i in the bag \mathbf{X} , and then aggregates the embeddings as a weighted average. However, this approach still assumes that instances are independent because the attention weights are computed independently for each instance.

2.2 Self-attention

The self-attention mechanism was originally introduced by Vaswani et al. [13] as a tool for modelling long-range dependencies in sequential data, though it can equally be applied to permutation-invariant data, such as instances in a bag. An attention head operates on a set of input vectors $\{\mathbf{x}_1, \mathbf{x}_2, \dots, \mathbf{x}_n\}$ where each $\mathbf{x}_i \in \mathbb{R}^{d_x}$ and computes a set of the same number of output vectors $\{\mathbf{z}_1, \mathbf{z}_2, \dots, \mathbf{z}_n\}$, each $\mathbf{z}_i \in \mathbb{R}^{d_z}$. However, the dimensionality of the input vectors d_x and output vectors d_z may differ.

A particular output vector \mathbf{z}_i is computed as a weighted sum of linearly transformed input vectors \mathbf{x}_j ,

$$\mathbf{z}_i = \sum_{j=1}^n \alpha_{ij} (\mathbf{x}_j \mathbf{W}^V), \quad (6)$$

where the linear transformation is parameterised by a weight matrix $\mathbf{W}^V \in \mathbb{R}^{d_x \times d_z}$. The coefficients in the weighted sum α_{ij} are computed as a softmax over the compatibilities e_{ij} . The term e_{ij}

expresses the compatibility between input vectors \mathbf{x}_i and \mathbf{x}_j , and is computed as a dot product between the two vectors after each is transformed by a separate linear function:

$$e_{ij} = \frac{(\mathbf{x}_i \mathbf{W}^Q)(\mathbf{x}_j \mathbf{W}^K)^\top}{\sqrt{d_z}}. \quad (7)$$

These linear transformations are parameterized by two more weight matrices $\mathbf{W}^Q, \mathbf{W}^K \in \mathbb{R}^{d_x \times d_z}$. Intuitively, \mathbf{x}_j undergoes a linear transformation via \mathbf{W}^K to emit a key vector, which is compared to the query vector obtained by transforming \mathbf{x}_i via \mathbf{W}^Q .

Positional and spatial information On its own, the self-attention mechanism is permutation invariant. For sequential data (one-dimensional in the sense that there is only a temporal dimension), this issue was already addressed in the original transformer model [13] by adding a positional encoding $\mathbf{p}_i \in \mathbb{R}^{d_x}$ to each input vector \mathbf{x}_i before applying the self-attention mechanism. On the other hand, Shaw et al. [32] propose using relative position representations by adding learned representations to the key and value vectors of Eqs. (6) and (7) that depend on the relative distances between input tokens. Liutkus et al. [33] take this idea further to make it linear in complexity.

The 2D case, which is the focus of our paper, is more challenging because the input vectors \mathbf{x}_i are not ordered in a sequence, but rather associated with 2D coordinates. A simple approach is to perform the original positional encoding [13] separately on the x and y coordinates of each input element, and to then concatenate the resulting vectors [22, 34–36]. However, the dot product of two such positionally encoded vectors is no longer proportional to the ℓ_2 distance between the two locations, meaning that this information is lost. The solution proposed by [37] is a learned relative positional encoding using Fourier features, which retains the ℓ_2 distance information in the dot product.

However, instead of using a form of absolute 2D positional encoding, our approach directly incorporates relative distance information in the self-attention mechanism by adding a learned distance-dependent bias term to the attention weights in the compatibility function Eq. (7). In the literature, approaches involving a bias term in the attention weights have only been studied in the context of discrete distances [38, 39], while we consider continuous distances. In graph representation problems, Ying et al. [38] add a bias to the attention weights in the transformer using a trainable scalar. Perhaps the most similar approach to ours is that of Wu et al. [39], who propose variations of relative positional representations [32] for patch-based self-attention in image classification. Nonetheless, their approach is limited to discrete distance values because they split the input image into a regular grid of patches, while we consider patches where there are no such restrictions.

2.3 Self-attention in multiple instance learning

As mentioned earlier, many practical MIL problems require the consideration of more than one instance in a bag for a decision to be made which is in contrast to the original assumption in Eq. (1). Consequently, a new class of MIL models is emerging where the i.i.d. assumption of the patches is relaxed by an aggregation function that has the ability to consider dependencies between instances in the bag. The self-attention mechanism is particularly well-suited for this task, however, other models such as graph neural networks (GNNs) [40] have also been considered in this context.

A number of recent MIL models employ self-attention in the aggregation function [14–25] to capture dependencies between input tokens in a sequence, which in the case of MIL are instances in a bag. Interestingly, almost all of them are designed to operate on image patches, which is the focus of our work. These approaches consistently outperform classical MIL models operating under the patch independence assumption. Some approaches regard a bag simply as a set of image patches, ignoring their spatial arrangement altogether [14–18], however, this information may be crucial, especially in the medical domain. Approaches that do incorporate spatial information typically employ absolute positional encodings [20–25], though recently there has been work on using positional hierarchies [19]. However, to the best of our knowledge, there has been no work on using relative positional representations in MIL, which our focus herein.

3 DAS-MIL

Our model follows the three-step embedding-based MIL approach described in Section 2.1. First, We parameterise the feature extractor \mathbf{h} in Eq. (3) using a convolutional neural network (CNN) whose flattened outputs pass through a linear layer with d_z output units. Each image patch is processed

independently by the CNN to produce a feature vector $\mathbf{z}_i \in \mathbb{R}^{d_z}$ for each patch i . Secondly, we apply a novel type of self-attention which we term *distance-aware self-attention*, described in the next section, to the \mathbf{z}_i to obtain a new set of feature vectors $\mathbf{z}'_i \in \mathbb{R}^{d_z}$,

$$\{\mathbf{z}'_1, \mathbf{z}'_2, \dots, \mathbf{z}'_n\} = \text{DASAtt}(\{\mathbf{z}_1, \mathbf{z}_2, \dots, \mathbf{z}_n\}, \mathbf{D}) \quad (8)$$

based on the distance matrix $\mathbf{D} \in \mathbb{R}^{n \times n}$ whose (i, j) -th entry is the distance between the i -th and j -th patch δ_{ij} . Then, we aggregate the new feature vectors \mathbf{z}'_i to a single vector $\hat{\mathbf{z}} \in \mathbb{R}^{d_z}$ by computing the maximum value along each dimension such that the j -th element of $\hat{\mathbf{z}}$ is given by

$$\hat{z}_j = \max_{1 \leq i \leq n} z'_{i,j} \quad (9)$$

where $z'_{i,j}$ is the j -th component of \mathbf{z}'_i . Together, Eqs. (8) and (9) form the aggregation function \mathbf{g} in Eq. (3). Finally, we use the aggregated feature vector $\hat{\mathbf{z}}$ to compute the MIL score using a linear layer with a single output unit. Specifically, we parameterise the scoring function f in Eq. (3) as

$$S(\mathbf{X}) = f(\hat{\mathbf{z}}) = \sigma(\hat{\mathbf{z}}\mathbf{w}^S + b^S) \quad (10)$$

with weight and bias parameters $\mathbf{w}^S \in \mathbb{R}^{d_z}$ and $b^S \in \mathbb{R}$, respectively, and sigmoid activation σ .

We train the model end-to-end using a weighted version of the binary cross-entropy loss that accounts for class imbalances in the training set. The model is presented one bag at a time (*i.e.* in a batch of size one) with the loss for a particular bag \mathbf{X} and associated label Y computed as:

$$\mathcal{L} = -\omega Y \log S(\mathbf{X}) - (1 - Y) \log(1 - S(\mathbf{X})) \quad (11)$$

where the weight $\omega \in \mathbb{R}$ is the ratio of negative to positive bags in the training set.

3.1 Distance-aware self-attention

The central component of our model is the distance-aware self-attention mechanism. We retain the notation from Section 2.2 in that the self-attention mechanism acts on a set of input vectors $\mathbf{x}_1, \mathbf{x}_2, \dots, \mathbf{x}_n$, transforming them into a set of output vectors $\mathbf{z}_1, \mathbf{z}_2, \dots, \mathbf{z}_n$, which is consistent with the literature [13, 32, 39]. This is not to be confused with the notation in Section 3, where the input vectors to the self-attention mechanism are embedding vectors, already denoted as \mathbf{z}_i by convention in the MIL literature [12]; thus the output vectors were denoted as \mathbf{z}'_i above.

We first describe a general framework for incorporating relative distance information in self-attention, and then introduce our method as an instantiation of this framework in the next section. We then compare our method to existing work [32, 39, 41–44] in Section 3.1.2.

The general framework introduces three terms into the self-attention mechanism, $\mathbf{b}_{ij}^K, \mathbf{b}_{ij}^Q \in \mathbb{R}^{d_x}$ and $\mathbf{b}_{ij}^V \in \mathbb{R}^{d_z}$. Intuitively, these are learned representations of the relative distances between the i -th and j -th input elements. We add $\mathbf{b}_{ij}^V \in \mathbb{R}^{d_z}$ in the computation of the output vector \mathbf{z}_i from Eq. (6) as

$$\mathbf{z}_i = \sum_{j=1}^n \alpha_{ij} (\mathbf{x}_j \mathbf{W}^V + \mathbf{b}_{ij}^V). \quad (12)$$

In the compatibility function in Eq. (7), we add \mathbf{b}_{ij}^K to the key vector $\mathbf{x}_j \mathbf{W}^K$ in order to infuse distance information into the computation of the attention weights (and analogously \mathbf{b}_{ij}^Q):

$$e_{ij} = \frac{(\mathbf{x}_i \mathbf{W}^Q + \mathbf{b}_{ij}^Q)(\mathbf{x}_j \mathbf{W}^K + \mathbf{b}_{ij}^K)^\top - \mathbf{b}_{ij}^Q \mathbf{b}_{ij}^{K\top}}{\sqrt{d_z}}. \quad (13)$$

Efficient implementation There are two reasons for subtracting the term $\mathbf{b}_{ij}^Q \mathbf{b}_{ij}^{K\top}$ in Eq. (13). It improves the performance of our model (as we show in an ablation study) and saves some computation in the implementation of the compatibility function, as we explain next. When we rewrite Eq. (13) as

$$e_{ij} = \frac{(\mathbf{x}_i \mathbf{W}^Q)(\mathbf{x}_j \mathbf{W}^K)^\top + (\mathbf{x}_i \mathbf{W}^Q) \mathbf{b}_{ij}^{K\top} + (\mathbf{x}_j \mathbf{W}^K)^\top \mathbf{b}_{ij}^Q}{\sqrt{d_z}}, \quad (14)$$

the term $\mathbf{b}_{ij}^Q \mathbf{b}_{ij}^{K\top}$ cancels out. However, more importantly, we can precompute $(\mathbf{x}_i \mathbf{W}^Q)(\mathbf{x}_j \mathbf{W}^K)^\top$ for all pairs of input elements i, j as in the original self-attention mechanism [13], and store it in a matrix $\mathbf{A} \in \mathbb{R}^{n \times n}$. First, we calculate the matrix $\mathbf{X} \mathbf{W}^Q \in \mathbb{R}^{n \times d_z}$, where $\mathbf{X} \in \mathbb{R}^{n \times d_x}$ is the matrix whose rows are the input vectors \mathbf{x}_i . Similarly, we compute $\mathbf{X} \mathbf{W}^K \in \mathbb{R}^{n \times d_z}$. This gives rise to $\mathbf{A} = (\mathbf{X} \mathbf{W}^Q)(\mathbf{X} \mathbf{W}^K)^\top$ whose (i, j) -th element is the first term in Eq. (14). Furthermore, we can reuse the matrices $\mathbf{X} \mathbf{W}^Q$ and $\mathbf{X} \mathbf{W}^K$ in the computation of the other two terms.

3.1.1 Our method

Let δ_{ij} be the Euclidean distance between instances i and j . We define the relative positional encoding for the key vectors \mathbf{b}_{ij}^K as an interpolation between two learned vectors $\mathbf{u}^K, \mathbf{v}^K \in \mathbb{R}^{d_x}$:

$$\mathbf{b}_{ij}^K = \phi(\delta_{ij})\mathbf{u}^K + (1 - \phi(\delta_{ij}))\mathbf{v}^K, \quad (15)$$

where the interpolation coefficient $\phi(\delta)$ is obtained via a learned function $\phi: \mathbb{R} \rightarrow \mathbb{R}$ that maps the relative distance δ to a scalar. We parameterise ϕ as a sigmoid function that is scaled and shifted by learnable parameters $\beta, \theta \in \mathbb{R}$. Similarly, we define the encodings for \mathbf{b}_{ij}^Q and \mathbf{b}_{ij}^V as

$$\mathbf{b}_{ij}^Q = \phi(\delta_{ij})\mathbf{u}^Q + (1 - \phi(\delta_{ij}))\mathbf{v}^Q \quad \text{and} \quad \mathbf{b}_{ij}^V = \phi(\delta_{ij})\mathbf{u}^V + (1 - \phi(\delta_{ij}))\mathbf{v}^V, \quad (16)$$

using different trainable vectors $\mathbf{u}^Q, \mathbf{v}^Q \in \mathbb{R}^{d_x}$ and $\mathbf{u}^V, \mathbf{v}^V \in \mathbb{R}^{d_z}$. However, we find it beneficial to share the parameters β and θ of the ϕ function between all three encoding vectors $\mathbf{b}_{ij}^K, \mathbf{b}_{ij}^Q, \mathbf{b}_{ij}^V$.

More formally, the procedure outlined in this section gives rise to the distance-aware self-attention operator as it is used in Eq. (8), which computes a set of output vectors \mathbf{z}_i based on the input vectors \mathbf{x}_i and their relative distances δ_{ij} packed into a distance matrix $\mathbf{D} \in \mathbb{R}^{n \times n}$:

$$\text{DASAtt}(\{\mathbf{x}_1, \mathbf{x}_2, \dots, \mathbf{x}_n\}, \mathbf{D}) = \{\mathbf{z}_1, \mathbf{z}_2, \dots, \mathbf{z}_n\}. \quad (17)$$

3.1.2 Prior work

Adding distance dependent terms to the key vectors in Eq. (13) and the output vectors in Eq. (12) was first proposed by Shaw et al. [32] in the context of machine translation. The authors learn a relative position representation vector $\mathbf{r}_k^K \in \mathbb{R}^{d_z}$ for every relative distance $k \in \mathbb{Z}$ between input token positions (up to some maximum distance k_{\max} such that $|k| \leq k_{\max}$) and set $\mathbf{b}_{ij}^K = \mathbf{r}_{i-j}^K$. The same procedure is followed for \mathbf{b}_{ij}^V , with the difference that the query vector is not altered, *i.e.* $\mathbf{b}_{ij}^Q = \mathbf{0}$. However, note that the original work [32], as well as some of the other methods that followed [41, 42] (a comprehensive overview is provided by Wu et al. [39]), study the 1D case of language modelling where relative distances are discrete values representing token offsets.

There is some prior work on extending relative position representations to 2D images, where the image is split into a regular grid of tiles constituting the input elements. One approach is to compute separate relative position representations in the horizontal and vertical directions, and then either to concatenate them [43] or use them sequentially in consecutive layers [44] to form the final representation. However, this approach is not rotationally invariant, and cannot accurately compare relative distances in non-cardinal directions. This may not be a problem in the case of natural images, but it is an important consideration for medical images as they lack a canonical orientation and accurately capturing relative distances between biological structures may be crucial for the task.

Wu et al. [39] propose several relative position encodings designed specifically for images. The main idea is to discretise the relative Euclidean distances between input elements into a finite number of bins, and then learn a separate relative position representation for each bin. For k bins, the authors learn k relative position representation vectors $\mathbf{r}_1^V, \mathbf{r}_2^V, \dots, \mathbf{r}_k^V \in \mathbb{R}^{d_z}$ and then set $\mathbf{b}_{ij}^K = \mathbf{r}_b$ where b is the index of the bin containing the relative distance δ_{ij} . The same procedure is followed for \mathbf{b}_{ij}^Q and \mathbf{b}_{ij}^V . This approach is the most similar to ours because it is rotationally invariant by incorporating Euclidean distance information into the self-attention mechanism. However, like all of the other aforementioned relative position schemes, Wu et al. [39] did not consider the problem of MIL. Instead, they studied the situation where the input images were of a fixed size and split into a regular grid of tiles, so the relative distances were discrete values representing offsets between tiles. However, in MIL there is no such restriction, and especially in the medical domain, images may be of different sizes, patches could be sampled from anywhere in the image, and they need not be sampled exhaustively. Discretising the relative distances into bins may be problematic in MIL because the number of bins is a hyperparameter that needs to be tuned. If the number of bins is too small, the model cannot make distinctions between distances at the resolution required for the task at hand. If the number of bins is too large, the model will fail to generalise to unseen distances that were not present in the training set. In their setting, the input images were of fixed size, and the patches were exhaustively sampled from a regular grid, so the model could be trained to learn the relative position representations for all possible distances. This is not possible in MIL because there is no restriction on the number of possible distances, and the model must generalise to unseen distance values. Furthermore, Wu

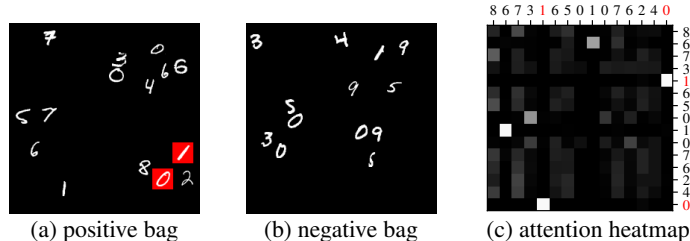


Figure 2: Two bags from the MNIST-COLLAGE test set. **(a)** The key instances in the positive bag are in red. Note that the bag actually contains two instances of “0” and two instances of “1”, but only the highlighted instances are actually close enough to each other to be considered a positive bag. **(b)** In the negative bag, the “0” and “1” are too far apart for a positive label. Note that negative bags do not necessarily need to even contain “0” and “1”. **(c)** Attention heatmap of DAS-MIL with key and query embeddings applied to the positive bag. Key instances are in red.

et al.’s model receives no explicit notion of ordering regarding the bins, so it must learn to infer this implicitly. Our approach does not suffer from these issues, because it operates on continuous distances and explicitly encodes the ordering of the distances via the ϕ function in Eq. (15).

4 Experiments and results

4.1 Toy dataset based on MNIST

Alongside their model, Ilse et al. [12] introduced a toy MIL problem based on the MNIST dataset [45] which they call MNIST-BAGS. In this dataset, each bag is comprised of a variable number of MNIST digits, *i.e.* instances. The bag label is positive if and only if it contains the digit “9” at least once. Due to its size and simplicity, this dataset lends itself particularly well to studying the behaviour of MIL models [18, 40]. However, MNIST-BAGS still operates under the classical MIL assumption that just one instance contributes to the bag label, so a variant of this dataset has been used where the bag label is positive if and only if it contains a pair of two specific digits, e.g. “7” and “9” [18, 46].

We extend this idea to a new dataset called MNIST-COLLAGE that incorporates the notion of relative distances by arranging the digits in a larger image, as shown in Fig. 2. Each bag is a collage of n digits, where n is sampled from a Gaussian distribution and rounded to the nearest integer. The digits locations are sampled from a uniform distribution encompassing the dimensions of the collage and ensuring there is no overlap. We label a bag positive if and only if it contains a “0” and a “1” whose centroids are within a certain Euclidean distance of each other. Our training and test sets contain 300 and 100 bags, respectively, with the digits chosen randomly from the respective MNIST training and test sets, ensuring that exactly half of the bags in each set are positive. To further increase the difficulty of the problem, we also study an inverted version of this dataset (MNIST-COLLAGE-INV), where the relative distance must *exceed* a certain threshold.

Experimental setup We compare the performance of our approach to a number of existing MIL models, namely AB-MIL [12], MIL-GNN [40], and TransMIL [20]. Additionally, we apply existing models mentioned in Section 2 that were not specifically designed for MIL to the general MIL framework outlined in Section 2.1 by parameterising the aggregation function g in Eq. (3) with the specified model. In this regard, we evaluate the Set Transformer [47], a simple self-attention layer [13], as well as self-attention with various positional encodings [37, 43]. Importantly, we also evaluate self-attention with Wu et al.’s discrete relative position representations [39] (with 10 encodings) as described at the end of Section 3.1.2.

The same CNN architecture is used for feature extraction in all models, detailed in Appendix A. For each model, we perform a grid search over the learning rate, weight decay, and other model-specific hyperparameters, and report the best results across 5 runs with different seeds. We train each model for 50 epochs with a batch size of 1 using the AdamW optimizer [48] on a consumer-grade CPU. For our model, a learning rate of 10^{-3} and weight decay of 10^{-2} achieved the best results.

Results Table 1 indicates that models that do not incorporate any positional information perform the worst, which is expected as the problem inherently requires the consideration of spatial correspondences. 12% of the samples in the test set are negative bags that contain at least one “0” and one

Table 1: Results on the MNIST-COLLAGE and MNIST-COLLAGE-INV datasets. We report the mean and standard deviation of the balanced accuracy score over 5 runs (AUROC is reported in Appendix A). Models that contain the word “with” in their name parameterise the aggregation function g in Eq. (3) with the specified model, but these models were not originally designed for MIL. All models employ the same CNN architecture for feature extraction and are trained end-to-end. The second column indicates the type of positional encoding used: absolute (ABS), relative (REL) or neither (\times).

Model	Pos	Params	MNIST-COLLAGE		MNIST-COLLAGE-INV	
			Train	Test	Train	Test
MIL with max pool	\times	15.6K	0.846 ± 0.021	0.828 ± 0.033	0.840 ± 0.009	0.788 ± 0.029
AB-MIL [12]	\times	16.1K	0.799 ± 0.014	0.740 ± 0.010	0.805 ± 0.006	0.692 ± 0.015
MIL-GNN [40]	REL	19.2K	0.686 ± 0.143	0.656 ± 0.123	0.784 ± 0.023	0.756 ± 0.019
MIL with iSet Transformer [47]	\times	22.1K	0.813 ± 0.017	0.734 ± 0.040	0.813 ± 0.023	0.720 ± 0.016
MIL with Set Transformer [47]	\times	17.6K	0.815 ± 0.052	0.832 ± 0.041	0.819 ± 0.018	0.792 ± 0.045
MIL with SA [13]	\times	17.2K	0.881 ± 0.013	0.848 ± 0.024	0.840 ± 0.019	0.786 ± 0.077
MIL with SA + axial PE [43]	ABS	17.6K	0.862 ± 0.008	0.786 ± 0.051	0.902 ± 0.018	0.774 ± 0.015
MIL with SA + Fourier PE [37]	ABS	18.4K	0.878 ± 0.035	0.820 ± 0.022	0.879 ± 0.037	0.808 ± 0.029
MIL with disc. rel. SA [39]	REL	17.8K	0.921 ± 0.014	0.926 ± 0.030	0.877 ± 0.031	0.846 ± 0.060
TransMIL [20]	ABS	2.18M	0.957 ± 0.029	0.728 ± 0.054	0.957 ± 0.015	0.742 ± 0.053
DAS-MIL (ours)	REL	17.4K	0.955 ± 0.011	0.958 ± 0.013	0.953 ± 0.004	0.906 ± 0.034

“1” which means that a model could achieve an accuracy of 88% by ignoring the spatial information, (in effect, this task would be identical to the MNIST-BAGS dataset with two key instances [18, 46]). While it is self-evident why the models without positional information do not exceed this score, it is important to note that none of the models that employ absolute positional encodings perform better than this baseline. This indicates that models with absolute positional encodings have trouble comparing relative distances between instances, which is not surprising because the absolute positional encodings are not rotationally invariant. TransMIL [20] uses a type of absolute positional encoding where features are aggregated in a pyramid, and while this mechanism achieves the best training accuracy, it does not generalise well, which may be explained by the fact that their model has two orders of magnitude more parameters than all the others. In general, models perform worse on MNIST-COLLAGE-INV, which is expected as long-range dependencies need to be considered. Still, our model achieves the best test accuracy on both datasets, and is the only model that achieves a test accuracy of over 90% on MNIST-COLLAGE-INV. The discrete relative self-attention mechanism achieved the second best results, however, it uses 10 embeddings while our model uses just two.

Embeddings We perform an ablation study to assess how much each of the three embedding terms $b_{ij}^K, b_{ij}^Q, b_{ij}^V$ in Eqs. (12) and (13) contribute to our model’s performance. Testing all combinations of setting the embedding terms to zero, we find that our model performs worst when using just the key embeddings (*i.e.* $b_{ij}^Q = b_{ij}^V = \mathbf{0}$), and best when using all three embeddings on MNIST-COLLAGE. However, on MNIST-COLLAGE-INV, the model without query embeddings actually exhibits slightly better generalisation ability. Note that setting all three embeddings to zero would reduce the model to a simple self-attention layer, which performed much worse (see Table 1). Furthermore, we study the effect of the term $b_{ij}^Q b_{ij}^{K\top}$ in Eq. (13) by comparing the performance of our model with and without it, and find that its subtraction improves the test accuracy by 1% on both datasets. As remarked in Section 3.1, this term also saves some computation in the compatibility function. Finally, we assess whether the embedding vectors ($u^K, v^K, u^Q, v^Q, u^V, v^V$ in Eqs. (15) and (16)) even need to be learned, by randomly initialising and freezing them. Surprisingly, this decreases the mean test accuracy of our model by just 0.6% on MNIST-COLLAGE and 1% on MNIST-COLLAGE-INV (albeit with a larger standard deviation), indicating that the model is not very sensitive to the actual values of the embedding vectors. However, the two trainable scalars β and θ of the $\phi(\cdot)$ function in Eq. (15) are crucial; keeping them fixed or replacing $\phi(\cdot)$ with the identity function results in significantly worse performance. The results of these ablation studies are summarised in Table 6 of Appendix A.

Interpreting attention maps We can visualise the attention weights α_{ij} as a heatmap to gain insight into the model’s behaviour. The attention weights are computed via the compatibility function from Eq. (13) which incorporates distance information via the query and key embeddings. However, the value embeddings are added to the output vectors from Eq. (12) after the attention weights have been computed, so their effect is not as straightforward to interpret. Therefore, we visualise the attention weights of the version of our model that does not use value embeddings, *i.e.* $b_{ij}^V = \mathbf{0}$ in the ablation study above. Figure 2c shows the attention heatmap of this model applied to the positive bag depicted in Fig. 2a. This bag is interesting because it contains multiple instances of the digits “0” and “1”, but only the two instances highlighted in red are close enough to be considered a positive bag. In

Table 2: Results on the CAMELYON16 dataset.

Model	Pos	Params	AUROC		Balanced accuracy	
			Train	Test	Train	Test
MIL with max pool	\times	769	0.686 ± 0.018	0.739 ± 0.017	0.639 ± 0.033	0.573 ± 0.077
AB-MIL [12]	\times	8.47K	0.964 ± 0.003	0.795 ± 0.009	0.923 ± 0.004	0.773 ± 0.010
MIL with SA [13]	\times	27.7K	0.972 ± 0.014	0.823 ± 0.050	0.925 ± 0.016	0.803 ± 0.033
MIL with SA + axial PE [43]	ABS	27.7K	0.956 ± 0.016	0.485 ± 0.018	0.887 ± 0.017	0.490 ± 0.034
MIL with SA + Fourier PE [37]	ABS	41K	0.975 ± 0.007	0.819 ± 0.028	0.932 ± 0.011	0.770 ± 0.041
MIL with disc. rel. SA [39]	REL	28K	0.976 ± 0.006	0.806 ± 0.015	0.926 ± 0.017	0.787 ± 0.008
TransMIL [20]	ABS	2.54M	0.999 ± 0.002	0.911 ± 0.027	0.997 ± 0.007	0.857 ± 0.032
DAS-MIL (ours)	REL	412K	0.997 ± 0.005	0.914 ± 0.007	0.978 ± 0.022	0.864 ± 0.025

the attention map, the two corresponding entries are highly activated. By contrast, other entries in the attention matrix corresponding to the other digits that are too far apart are not activated. Interestingly, there are two other cells that have a higher activation, corresponding to the pair of “6” and “1”, which may be explained by the similarly round shape of “6” and “0”.

4.2 The CAMELYON16 dataset

The CAMELYON16 dataset [31] consists of hematoxylin and eosin (H&E) stained slides of lymph node sections from breast cancer patients. Each slide is classified either as “tumour” (positive) or “normal” (negative), which is particularly challenging because large regions in the tumour slides contain normal tissue. We removed three slides that Liu et al. [49] identified as being labelled incorrectly, resulting in a training set of 111 tumour and 156 normal slides, and a test set of 48 tumour and 80 normal slides.

We extract patches at a resolution of 224×224 pixels from the slides in a regular grid, discarding patches that do not contain any tissue. Due to the heterogeneity of the slides (they were acquired at two different medical centres with different scanners), we apply Macenko et al.’s stain normalisation method [50] to each patch. The mean bag size is 4,004 in the train set, but we set the maximum bag size to 6,000 to reduce the memory requirements of the model (in larger bags, we randomly sample 6,000 patches). We then extract a 768-dimensional feature vector from each patch using a Transformer model that was trained on a large dataset of H&E stained patches [51]. This transformer corresponds to the feature extractor h in Eq. (3), with the difference that it is not trained end-to-end with the rest of the model; instead, we use the pre-trained weights from the original work [51] throughout to reduce the training time (they need only be computed once for the whole dataset before training).

Like TransMIL [20], we add a trainable fully connected layer with ReLU activation at the start of our model to reduce the feature size from 768 to $d_z = 512$. To find the best hyperparameters for every model, we perform a grid search over the learning rate, weight decay, and optimizer (AdamW [48] or Lookahead [52]), training every model for 30 epochs and reporting the best results in Table 2. We find the best results with the Lookahead optimizer [52] in the tested models. On a single GPU, our model takes approximately three hours to train which is comparable to TransMIL [20] and the MIL variant that uses self-attention with discrete relative position representations [39]. The other models such as AB-MIL [12] and vanilla self-attention are much simpler and require about half that time, but do not achieve competitive results. For TransMIL [20], which in Shao et al.’s original work also uses the Lookahead optimizer, our hyperparameter search yielded the same optimal learning rate and weight decay as in their work, but we were unable to reproduce their reported results on CAMELYON16 (we achieve a test area under the receiver operating characteristic (AUROC) of 0.911 with their model compared to their reported 0.909). This may be due to differences in the preprocessing steps or due to the random seed (we report mean and standard deviation across 5 runs with different random seeds, but Shao et al. do not specify how many runs they performed or include the standard deviation in their results). While TransMIL achieves better AUROC and balanced accuracy scores on the training set, our model generalises better to the test set, where our model outperforms all other approaches.

5 Conclusion

Some image-based MIL problems, especially in the domain of medical imaging, require the model to consider the spatial arrangement of the tiles for prediction. Recognising this fact, we develop a self-attention-based MIL model that is able to compare relative distances using a novel scheme for relative distance representations. We validate our model on two datasets: a custom dataset designed

to test the ability to compare relative distances, and CAMELYON16. We have open-sourced the model’s code to ensure that our model can be employed and validated on more datasets.

Limitations and future work A limitation of our model is that it is interpretable only in certain configurations (*i.e.* without value embeddings). We leave improving the model’s interpretability for future work. Furthermore, it would be interesting to study variations of the interpolation function $\phi(x)$, and whether it could be used to incorporate inductive biases.

Broader impact We hope our models inspire the development of more relative distance-based approaches. As mentioned in the introduction, researchers in computational pathology have shown that spatial information is crucial for forming diagnoses in various problems, so relative distance-based approaches have the potential to improve diagnostic quality. In that vein, we would also encourage more research in the interpretability and safety of these models.

References

- [1] Thomas G Dietterich, Richard H Lathrop, and Tomás Lozano-Pérez. “Solving the multiple instance problem with axis-parallel rectangles”. In: *Artificial intelligence* 89.1-2 (1997), pp. 31–71.
- [2] Oded Maron and Tomás Lozano-Pérez. “A Framework for Multiple-Instance Learning”. In: *Advances in Neural Information Processing Systems*. Vol. 10. 1997.
- [3] Jiajun Wu et al. “Deep multiple instance learning for image classification and auto-annotation”. In: *Proceedings of the IEEE conference on computer vision and pattern recognition*. 2015, pp. 3460–3469.
- [4] Fang Wan et al. “C-mil: Continuation multiple instance learning for weakly supervised object detection”. In: *Proceedings of the IEEE/CVF Conference on Computer Vision and Pattern Recognition*. 2019, pp. 2199–2208.
- [5] Gang Fu et al. “Implementation of multiple-instance learning in drug activity prediction”. In: *BMC bioinformatics*. Vol. 13. 15. BioMed Central. 2012, pp. 1–12.
- [6] Nikolaos Pappas and Andrei Popescu-Belis. “Explaining the stars: Weighted multiple-instance learning for aspect-based sentiment analysis”. In: *Proceedings of the 2014 Conference on Empirical Methods In Natural Language Processing (EMNLP)*. 2014, pp. 455–466.
- [7] Gabriele Campanella et al. “Clinical-grade computational pathology using weakly supervised deep learning on whole slide images”. In: *Nature medicine* 25.8 (2019), pp. 1301–1309.
- [8] Jan Moritz Niehues et al. “Generalizable biomarker prediction from cancer pathology slides with self-supervised deep learning: A retrospective multi-centric study”. In: *Cell Reports Medicine* (2023), p. 100980. ISSN: 2666-3791.
- [9] Oliver Lester Saldanha et al. “Self-supervised attention-based deep learning for pan-cancer mutation prediction from histopathology”. In: *NPJ Precision Oncology* 7.1 (2023), p. 35.
- [10] Omar SM El Nahhas et al. “Regression-based Deep-Learning predicts molecular biomarkers from pathology slides”. In: *arXiv preprint arXiv:2304.05153* (2023).
- [11] Xinggang Wang et al. “Revisiting multiple instance neural networks”. In: *Pattern Recognition* 74 (2018), pp. 15–24.
- [12] Maximilian Ilse, Jakub Tomczak, and Max Welling. “Attention-based deep multiple instance learning”. In: *International conference on machine learning*. PMLR. 2018, pp. 2127–2136.
- [13] Ashish Vaswani et al. “Attention is all you need”. In: *Advances in neural information processing systems* 30 (2017).
- [14] Dawid Rymarczyk et al. “Kernel self-attention for weakly-supervised image classification using deep multiple instance learning”. In: *Proceedings of the IEEE/CVF Winter Conference on Applications of Computer Vision*. 2021, pp. 1721–1730.
- [15] Richard J Chen et al. “Multimodal co-attention transformer for survival prediction in gigapixel whole slide images”. In: *Proceedings of the IEEE/CVF International Conference on Computer Vision*. 2021, pp. 4015–4025.
- [16] Andriy Myronenko et al. “Accounting for dependencies in deep learning based multiple instance learning for whole slide imaging”. In: *Medical Image Computing and Computer Assisted Intervention—MICCAI 2021: 24th International Conference, Strasbourg, France, September 27–October 1, 2021, Proceedings, Part VIII* 24. 2021, pp. 329–338.
- [17] Bin Li and Kevin W Eliceiri. “Dual-stream maximum self-attention multi-instance learning”. In: *arXiv preprint arXiv:2006.05538* (2020).

- [18] Zhenliang Li et al. “Deep multi-instance learning with induced self-attention for medical image classification”. In: *2020 IEEE International Conference on Bioinformatics and Biomedicine (BIBM)*. 2020, pp. 446–450.
- [19] Conghao Xiong et al. “Diagnose Like a Pathologist: Transformer-Enabled Hierarchical Attention-Guided Multiple Instance Learning for Whole Slide Image Classification”. In: *arXiv preprint arXiv:2301.08125* (2023).
- [20] Zhuchen Shao et al. “Transmil: Transformer based correlated multiple instance learning for whole slide image classification”. In: *Advances in neural information processing systems* 34 (2021), pp. 2136–2147.
- [21] Sophia J. Wagner et al. “Fully transformer-based biomarker prediction from colorectal cancer histology: a large-scale multicentric study”. In: *arXiv preprint arXiv:2301.09617* (2023).
- [22] Ziwang Huang et al. “Integration of patch features through self-supervised learning and transformer for survival analysis on whole slide images”. In: *Medical Image Computing and Computer Assisted Intervention–MICCAI 2021: 24th International Conference, Strasbourg, France, September 27–October 1, 2021, Proceedings, Part VIII* 24. 2021, pp. 561–570.
- [23] Richard J Chen et al. “Scaling vision transformers to gigapixel images via hierarchical self-supervised learning”. In: *Proceedings of the IEEE/CVF Conference on Computer Vision and Pattern Recognition*. 2022, pp. 16144–16155.
- [24] Ziniu Qian et al. “Transformer based multiple instance learning for weakly supervised histopathology image segmentation”. In: *Medical Image Computing and Computer Assisted Intervention–MICCAI 2022: 25th International Conference, Singapore, September 18–22, 2022, Proceedings, Part II*. Springer. 2022, pp. 160–170.
- [25] Yi Ding et al. “Deep Multi-Instance Learning with Adaptive Recurrent Pooling for Medical Image Classification”. In: *2022 IEEE International Conference on Bioinformatics and Biomedicine (BIBM)*. IEEE. 2022, pp. 3335–3342.
- [26] Ines P Nearchou et al. “Automated Analysis of Lymphocytic Infiltration, Tumor Budding, and Their Spatial Relationship Improves Prognostic Accuracy in Colorectal Cancer Automated Image Analysis in Colorectal Cancer Prognosis”. In: *Cancer immunology research* 7.4 (2019), pp. 609–620.
- [27] Charlotte M. Jones-Todd et al. “Identifying prognostic structural features in tissue sections of colon cancer patients using point pattern analysis”. In: *Statistics in Medicine* 38.8 (2019), pp. 1421–1441.
- [28] Raffaele De Filippis et al. “Use of high-plex data reveals novel insights into the tumour microenvironment of clear cell renal cell carcinoma”. In: *Cancers* 14.21 (2022), p. 5387.
- [29] Hubert Hackl et al. “Computational genomics tools for dissecting tumour–immune cell interactions”. In: *Nature Reviews Genetics* 17.8 (2016), pp. 441–458.
- [30] Sarah E Shelton et al. “Engineering approaches for studying immune-tumor cell interactions and immunotherapy”. In: *Isience* 24.1 (2021), p. 101985.
- [31] Babak Ehteshami Bejnordi et al. “Diagnostic assessment of deep learning algorithms for detection of lymph node metastases in women with breast cancer”. In: *JAMA* 318.22 (2017), pp. 2199–2210.
- [32] Peter Shaw, Jakob Uszkoreit, and Ashish Vaswani. “Self-Attention with Relative Position Representations”. In: *North American Chapter of the Association for Computational Linguistics*. 2018.
- [33] Antoine Liutkus et al. “Relative positional encoding for transformers with linear complexity”. In: *International Conference on Machine Learning*. PMLR. 2021, pp. 7067–7079.
- [34] Nicolas Carion et al. “End-to-end object detection with transformers”. In: *Computer Vision–ECCV 2020: 16th European Conference, Glasgow, UK, August 23–28, 2020, Proceedings, Part I* 16. 2020, pp. 213–229.
- [35] Alexey Dosovitskiy et al. “An Image is Worth 16x16 Words: Transformers for Image Recognition at Scale”. In: *International Conference on Learning Representations*. 2021.
- [36] Niki Parmar et al. “Image transformer”. In: *International conference on machine learning*. 2018, pp. 4055–4064.
- [37] Yang Li et al. “Learnable Fourier Features for Multi-dimensional Spatial Positional Encoding”. In: *Advances in Neural Information Processing Systems*. Vol. 34. 2021, pp. 15816–15829.
- [38] Chengxuan Ying et al. “Do Transformers Really Perform Badly for Graph Representation?”. In: *Advances in Neural Information Processing Systems*. Vol. 34. 2021, pp. 28877–28888.

- [39] Kan Wu et al. “Rethinking and improving relative position encoding for vision transformer”. In: *Proceedings of the IEEE/CVF International Conference on Computer Vision*. 2021, pp. 10033–10041.
- [40] Ming Tu et al. “Multiple instance learning with graph neural networks”. In: *arXiv preprint arXiv:1906.04881* (2019).
- [41] Zihang Dai et al. “Transformer-XL: Attentive Language Models beyond a Fixed-Length Context”. In: *Proceedings of the 57th Annual Meeting of the Association for Computational Linguistics*. Florence, Italy: Association for Computational Linguistics, June 2019, pp. 2978–2988.
- [42] Zhiheng Huang et al. “Improve Transformer Models with Better Relative Position Embeddings”. In: *Findings of the Association for Computational Linguistics: EMNLP 2020*. Association for Computational Linguistics, Nov. 2020, pp. 3327–3335.
- [43] Prajit Ramachandran et al. “Stand-Alone Self-Attention in Vision Models”. In: *Advances in Neural Information Processing Systems*. Ed. by H. Wallach et al. Vol. 32. Curran Associates, Inc., 2019.
- [44] Huiyu Wang et al. “Axial-DeepLab: Stand-Alone Axial-Attention for Panoptic Segmentation”. In: *European Conference on Computer Vision (ECCV)*. 2020.
- [45] Li Deng. “The mnist database of handwritten digit images for machine learning research [best of the web]”. In: *IEEE signal processing magazine* 29.6 (2012), pp. 141–142.
- [46] Lu Zhao et al. “Generalized attention-based deep multi-instance learning”. In: *Multimedia Systems* 29.1 (2023), pp. 275–287.
- [47] Juho Lee et al. “Set transformer: A framework for attention-based permutation-invariant neural networks”. In: *International conference on machine learning*. PMLR. 2019, pp. 3744–3753.
- [48] Ilya Loshchilov and Frank Hutter. “Decoupled Weight Decay Regularization”. In: *International Conference on Learning Representations*. 2019.
- [49] Yun Liu et al. “Detecting cancer metastases on gigapixel pathology images”. In: *arXiv preprint arXiv:1703.02442* (2017).
- [50] Marc Macenko et al. “A method for normalizing histology slides for quantitative analysis”. In: *IEEE international symposium on biomedical imaging*. 2009, pp. 1107–1110.
- [51] Xiyue Wang et al. “Transformer-based unsupervised contrastive learning for histopathological image classification”. In: *Medical Image Analysis* 81 (2022), p. 102559.
- [52] Michael Zhang et al. “Lookahead optimizer: k steps forward, 1 step back”. In: *Advances in neural information processing systems* 32 (2019).
- [53] Petar Veličković et al. “Graph Attention Networks”. In: *International Conference on Learning Representations*. 2018.
- [54] Thomas N. Kipf and Max Welling. “Semi-Supervised Classification with Graph Convolutional Networks”. In: *International Conference on Learning Representations*. 2017.

A Details of the MNIST-COLLAGE experiments

In the experiments involving the MNIST-COLLAGE and MNIST-COLLAGE-INV datasets, we use a CNN as the feature extractor h in Eq. (3). Each model is trained end-to-end, *i.e.* the feature extractor is trained alongside the rest of the model, and they all use the same CNN architecture, described as follows: a convolutional layer (10 output channels, kernel size 5, stride 1), ReLU activation, max pooling (kernel size 2, stride 2), dropout (probability 0.1); another convolutional layer (20 output channels, kernel size 5, stride 1), ReLU activation, max pooling (kernel size 2, stride 2); the flattened outputs are then passed through a dropout layer (probability 0.5) and a linear layer (32 output units) activated by ReLU. This means that we employ a feature size $d_z = 32$ using the notation from Section 2.1.

Hyperparameters The best hyperparameters found in the grid search are shown in Table 3 for each model on the MNIST-COLLAGE dataset. One of the hyperparameters we considered was the final part of the feature aggregation function g which in Eq. (9) is the maximum function. We find that every model’s best hyperparameter configuration uses max instead of mean pooling, including the GNNs, where the tested aggregation functions were global mean and global max pooling. It makes sense that max pooling is more suitable for MIL because just a small number of key instances are responsible for the bag label, so the corresponding features may be diluted by mean pooling.

Table 3: Best hyperparameters found via grid search for each model on the MNIST-COLLAGE dataset.

Model	optimiser	LR	weight decay	hidden dim	agg
MIL with max pool	Adam	0.0001	0.01	10	max
AB-MIL [12]	Adam	0.0001	0.001	15	N/A
MIL with GNN (GAT [53])	Adam	0.001	0.1	20	max
MIL with GNN (GCN [54])	Adam	0.001	0.1	15	max
MIL-GNN [40]	Adam	0.001	0.01	20	N/A
MIL with iSet Transformer [47]	Adam	0.0001	0.1	15	N/A
MIL with Set Transformer [47]	Adam	0.001	0.1	10	N/A
MIL with SA [13]	Adam	0.001	0.1	10	max
MIL with SA + axial PE [43]	Adam	0.0001	0.1	15	max
MIL with SA + Fourier PE [37]	Adam	0.001	0.001	15	max
MIL with disc. rel. SA [39]	Adam	0.0001	0.1	10	max
TransMIL [20]	Lookahead	0.0001	0.1	N/A	N/A
DAS-MIL (ours)	Adam	0.001	0.01	10	max

Further results For completeness, we report the results of experiments we conducted using MIL with two different types of GNNs (employing GAT [53] or GCN [54] layers) in Table 4. We did not include these results in the main paper to avoid cluttering Table 1. We also report the AUROC scores of the MNIST-COLLAGE and MNIST-COLLAGE-INV experiments in Table 5.

Table 4: Further results on the MNIST-COLLAGE and MNIST-COLLAGE-INV datasets (reporting balanced accuracy scores).

Model	Pos	Params	MNIST-COLLAGE		MNIST-COLLAGE-INV	
			Train	Test	Train	Test
MIL with GNN (GAT [53])	REL	16.7K	0.811 ± 0.089	0.758 ± 0.041	0.745 ± 0.033	0.716 ± 0.018
MIL with GNN (GCN [54])	REL	16.3K	0.865 ± 0.031	0.790 ± 0.058	0.883 ± 0.034	0.794 ± 0.036

Ablation study We report the results of the ablation study from Section 4.1 that investigated variants of the embeddings in Table 6.

B Details of the CAMELYON16 experiments

We performed the feature extraction as detailed in Section 4.2 once before training because it is computationally expensive and we chose the feature extractor to be non-trainable. The entire feature extraction pipeline (*i.e.* splitting the WSI into tiles, discarding tiles with too little tissue, performing stain normalisation, and extracting features) was performed using the

Table 5: AUROC scores on the MNIST-COLLAGE and MNIST-COLLAGE-INV datasets.

Model	Pos	Params	MNIST-COLLAGE		MNIST-COLLAGE-INV	
			Train	Test	Train	Test
MIL with max pool	\times	15.6K	0.924 \pm 0.007	0.905 \pm 0.008	0.912 \pm 0.008	0.830 \pm 0.010
AB-MIL [12]	\times	16.1K	0.893 \pm 0.017	0.825 \pm 0.008	0.890 \pm 0.012	0.790 \pm 0.008
MIL with GNN (GAT [53])	REL	16.7K	0.873 \pm 0.086	0.820 \pm 0.068	0.795 \pm 0.045	0.739 \pm 0.032
MIL with GNN (GCN [54])	REL	16.3K	0.932 \pm 0.029	0.851 \pm 0.033	0.941 \pm 0.027	0.886 \pm 0.013
MIL with iSet Transformer [47]	\times	22.1K	0.889 \pm 0.008	0.829 \pm 0.013	0.881 \pm 0.011	0.808 \pm 0.004
MIL with Set Transformer [47]	\times	17.6K	0.869 \pm 0.064	0.867 \pm 0.036	0.872 \pm 0.014	0.855 \pm 0.024
MIL-GNN [40]	REL	19.2K	0.648 \pm 0.022	0.708 \pm 0.059	0.723 \pm 0.056	0.716 \pm 0.071
MIL-GNN-DS [40]	REL	19.2K	0.771 \pm 0.130	0.778 \pm 0.093	0.864 \pm 0.027	0.817 \pm 0.008
MIL with SA [13]	\times	17.6K	0.945 \pm 0.035	0.853 \pm 0.041	0.933 \pm 0.063	0.816 \pm 0.074
MIL with SA + axial PE [43]	ABS	17.6K	0.941 \pm 0.011	0.860 \pm 0.063	0.963 \pm 0.005	0.877 \pm 0.015
MIL with SA + Fourier PE [37]	ABS	18.4K	0.943 \pm 0.025	0.874 \pm 0.012	0.939 \pm 0.034	0.863 \pm 0.016
MIL with disc. rel. SA [39]	REL	17.8K	0.970 \pm 0.005	0.975 \pm 0.005	0.954 \pm 0.031	0.923 \pm 0.089
TransMIL [20]	ABS	2.18M	0.991 \pm 0.009	0.831 \pm 0.041	0.993 \pm 0.004	0.805 \pm 0.046
DAS-MIL (ours)	REL	17.4K	0.990 \pm 0.003	0.992 \pm 0.009	0.991 \pm 0.002	0.970 \pm 0.020

Table 6: Results of varying the embeddings used in the DAS-MIL model. The first column indicates which embeddings are used, *i.e.* b^K for key embeddings, b^Q for query embeddings, and b^V for value embeddings as in Eqs. (12) and (13). Unused embeddings are set to zero, *i.e.* the model “DAS-MIL (b^K)” uses only key embeddings and sets $b^Q = b^V = \mathbf{0}$. In the fourth and eighth rows, we add the term $b_{ij}^Q (b_{ij}^K)^\top$ in the numerator of the compatibility function Eq. (14). The penultimate row shows the performance of our method if all embeddings are kept fixed, *i.e.* using non-trainable random vectors. The last row refers to the main DAS-MIL model described throughout the paper which uses all three trainable embeddings.

Model	Params	MNIST-COLLAGE		MNIST-COLLAGE-INV	
		Train	Test	Train	Test
DAS-MIL (b^K)	17.3K	0.929 \pm 0.059	0.910 \pm 0.029	0.870 \pm 0.073	0.836 \pm 0.077
DAS-MIL (b^Q)	17.3K	0.919 \pm 0.014	0.914 \pm 0.055	0.848 \pm 0.108	0.836 \pm 0.121
DAS-MIL (b^V)	17.3K	0.926 \pm 0.017	0.912 \pm 0.015	0.917 \pm 0.030	0.890 \pm 0.029
DAS-MIL (b^K, b^Q) (+ $b^Q b^K^\top$ in Eq. (14))	17.3K	0.899 \pm 0.051	0.906 \pm 0.065	0.907 \pm 0.043	0.850 \pm 0.062
DAS-MIL (b^K, b^Q)	17.3K	0.918 \pm 0.035	0.926 \pm 0.029	0.927 \pm 0.019	0.940 \pm 0.029
DAS-MIL (b^K, b^V)	17.3K	0.940 \pm 0.023	0.934 \pm 0.019	0.948 \pm 0.008	0.942 \pm 0.028
DAS-MIL (b^Q, b^V)	17.3K	0.927 \pm 0.015	0.916 \pm 0.013	0.954 \pm 0.012	0.912 \pm 0.026
DAS-MIL (b^K, b^Q, b^V) (+ $b^Q b^K^\top$ in Eq. (14))	17.4K	0.932 \pm 0.029	0.942 \pm 0.013	0.910 \pm 0.048	0.898 \pm 0.071
DAS-MIL (non-trainable b^K, b^Q, b^V)	17.3K	0.937 \pm 0.013	0.952 \pm 0.023	0.932 \pm 0.045	0.896 \pm 0.065
DAS-MIL (b^K, b^Q, b^V)	17.4K	0.955 \pm 0.011	0.958 \pm 0.013	0.953 \pm 0.004	0.906 \pm 0.034

open-source end2end-WSI-preprocessing tool available at <https://github.com/KatherLab/end2end-WSI-preprocessing>.